NASA TECHNICAL NOTE

NASA TN D-4793

DIVERGENCE OF SOME ALL-MOVABLE CONTROL SURFACES INCLUDING DRAG LOADINGS

by Robert C. Goetz

Langley Research Center
Langley Station, Hampton, Va.

NATIONAL AERONAUTICS AND SPACE ADMINISTRATION • WASHINGTON, D. C. • OCTOBER 1968

NASA TN D-4793

DIVERGENCE OF SOME ALL-MOVABLE CONTROL SURFACES INCLUDING DRAG LOADINGS

By Robert C. Goetz

Langley Research Center
Langley Station, Hampton, Va.

NATIONAL AERONAUTICS AND SPACE ADMINISTRATION

For sale by the Clearinghouse for Federal Scientific and Technical Information
Springfield, Virginia 22151 – CFSTI price $3.00

DIVERGENCE OF SOME ALL-MOVABLE CONTROL SURFACES INCLUDING DRAG LOADINGS

By Robert C. Goetz
Langley Research Center

SUMMARY

The aeroelastic divergence characteristics of some rigid all-movable control surfaces supported by a flexible shaft have been studied analytically, and the results have been compared with existing experimental data in the Mach number range from 1.64 to 15.4. The configuration studied was a blunt, double-wedge control surface supported by a long, thin cantilever that was weak in the lift direction and stiff in the drag direction.

The results of the study indicate that a new type of divergence instability is inherent to this configuration. Its character is a mode of deflection consisting of lateral bending accompanied by torsional rotation. The analysis and experiments indicate that drag loadings, in addition to lift loadings, are important in this new divergence instability. Estimates obtained from a potential-energy analysis using aerodynamic characteristics calculated from simple Newtonian theory were in fair agreement with the experimental results over the entire Mach number range; however, excellent agreement resulted when measured static aerodynamic derivatives were incorporated into the analysis for the Mach 6.8 and 15.4 experiments.

INTRODUCTION

Divergence is classically defined for unswept wings as a static instability of an airfoil in torsion, which occurs when the torsional rigidity of the structure is exceeded by aerodynamic twisting moments (ref. 1). However, a different type of divergence is possible for a rigid wing supported by a cantilevered shaft that is weak in the lift direction and stiff in the drag direction. When the drag loading is high, as for a wing with a blunt leading edge at high speeds, such a combination can diverge in a mode of deflection consisting of a twist accompanied by a lateral bending deflection. Whereas torsional divergence is analogous to the problem of column deflection with initial eccentricity (ref. 2), this two-degree-of-freedom instability is analogous to the lateral buckling of a beam. Although conventional all-movable control surfaces are supported on present-day vehicles by torque tubes with support bearings and therefore are not subject to this type of divergence instability, there is no assurance that mission requirements will not dictate design

changes on future generation vehicles. Additionally, there have been many aeroelastic investigations, especially flutter trend studies, where all-movable control-type models with integral support shafts were side-wall mounted for tunnel testing. (See, for example, refs. 3 to 8.) In two of these investigations (refs. 6 and 7), experimental divergence data are presented that were not predicted by conventional torsional divergence theory. It was these anomalous data that motivated the present investigation.

In the investigations of references 6 and 7, the model shaft was designed to give desired values of spanwise bending and torsional stiffnesses so as to insure flutter within the dynamic-pressure-range capability of the wind tunnels, and also to place the model out of the tunnel-wall boundary layer into the uniform flow region. These design criteria necessitated relatively long, thin rectangular shafts which, by their nature, are susceptible to divergence. Instabilities caused by static loadings have not been limiting design factors for models with similar structural arrangements in the past, since most aeroelastic investigations have been conducted at zero angle of attack and have employed low-drag (sharp-leading-edge) models. Consequently, the models experienced small static aerodynamic loadings during the tests. But with high-drag (blunt-leading-edge) designs, the static loadings have resulted in two-degree-of-freedom divergence.

Accordingly, the purpose of this paper is to investigate the two-degree-of-freedom divergence problem in general – including drag loadings – and the divergence characteristics of the model designs of references 6 and 7 in particular. A uniform cantilever shaft of thin rectangular cross section, coupled to a rigid panel at its free end and loaded by concentrated loads that simulate the aerodynamic forces of lift and drag on the panel, is discussed. The derivation of the equations governing the divergence instability is based on the potential-energy method applying the usual assumptions of elementary beam theory. Theoretical solutions of the divergence conditions are obtained for the applied loading conditions of lift only, drag only, and a combination of lift and drag. The final solution to the general problem of two applied loads is dependent upon such aerodynamic quantities as the magnitude of the drag force, the slope of the lift curve, and the location of the lift and drag forces on the panel. Newtonian theory aerodynamics are used to predict these steady-state aerodynamic parameters, and the results are compared with the experimental results of references 6 and 7. A theoretical parametric study is also conducted to determine the sensitivity of the divergence instability to these parameters. In addition, the same aerodynamic quantities were measured in the Langley hypersonic aeroelasticity tunnels at Mach numbers of 6.8 and 15.4, and the results are included in the divergence analysis, yielding additional divergence results for comparison.

SYMBOLS

a	spanwise distance from flexible-shaft—rigid-panel junction to applied loads
A	generalized amplitude
b	chordwise distance from elastic axis to applied drag load, positive forward
B_i	functions defined by equations (15) (i = 1, 2, 3, and 4)
c	panel chord
C	torsion rigidity; for a uniform beam with rectangular cross section, $C = \frac{ht^3}{3}\left(1 - 0.63\,\frac{t}{h}\right)G$
C_D	drag coefficient
C_L	lift coefficient
C_i	functions defined by equations (19) (i = 1, 2, 3, and 4)
C_{L_α}	slope of lift curve
d	chordwise distance from elastic axis to applied lift load, positive forward
D	drag
E	Young's modulus of elasticity
G	modulus of elasticity in shear
h	width of flexible shaft
I_Z	moment of inertia of cross section with respect to Z-axis
K_i	constants dependent upon structural quantities of flexible shaft, see equations (13)
l	length of flexible shaft

L	lift
L_ϕ	lift function, $L_\phi = \frac{L}{\phi_{x=l}}$
M	Mach number
M_X	bending moment about X-axis
M_Y	bending moment about Y-axis
M_Z	bending moment about Z-axis
M_{Z_1}	bending moment about Z_1-axis
q	dynamic pressure
q_i	generalized coordinate
S	rigid panel (planform) area
t	thickness of flexible shaft
U_B	strain energy of system in bending
U_T	total strain energy of system (see eq. (6))
U_ϕ	strain energy of system in torsion
v	free-stream velocity
V	total potential energy of system
x	spanwise coordinate measured from built-in end of shaft
x_o/c	chordwise location of aerodynamic center measured from leading edge, fraction chord
x_1	coordinate of an arbitrary cross section in deformed configuration which is tangent to elastic axis

y	lateral coordinate
y_1	coordinate at elastic axis of an arbitrary cross section in deformed configuration being in y principal direction
z	chordwise coordinate, positive aft, measured from elastic axis
z_1	coordinate at elastic axis of an arbitrary cross section in deformed configuration in z principal direction
X,Y,Z	fixed axes of undeformed-shaft configuration (see fig. 1)
X_1,Y_1,Z_1	axes of deformed-shaft configuration (see fig. 2)
α	angle of attack
δ_D	distance drag load moves in z-direction during deformation
μ	mass ratio (ratio of mass of model panel to mass of volume of test medium contained in a solid generated by revolving each chord about its midpoint, length of solid being wing semispan)
ρ	test-medium density
ϕ	angle of twist of shaft in deformed configuration relative to undeformed state
ω_n	frequency of nth mode (n = 1, 2, 3, . . .)
Ω_D	total work done on system by drag load
Ω_L	total work done on system by lift load

Subscripts:

calc	calculated
cr	critical (conditions at divergence)
div	divergence
D	due to drag

L	due to lift
max	maximum
meas	measured

DIVERGENCE ANALYSIS

Potential Energy of the System

The configuration to be analyzed is shown in figure 1. Here the x,y,z coordinate system is fixed in space, the origin coinciding with the fixed end of the support shaft axis. The origin of the x_1,y_1,z_1 coordinate system shown in figure 2 is taken at the elastic axis of an arbitrary cross section along the deformed shaft, with the Y_1- and Z_1-axes being in the principal directions of the section and the X_1-axis being in the direction of the tangent to the elastic axis. According to the condition imposed on the loads, forces shown in figure 1 remain in their initial directions while the shaft deforms.

The bending moment in the vertical plane at a distance x from the fixed end of the shaft is

$$M_Y = -D(\ell + a - x) \tag{1}$$

The component of this bending moment that is of interest is the one which causes bending about the Z_1-axis (see fig. 2(b)) and is

$$\left(M_{Z_1}\right)_D = -D(\ell + a - x)\sin\phi \tag{2a}$$

where ϕ denotes the angle of twist and is variable along the flexible shaft length. Similarly, the component of interest with respect to the Z_1-axis of the bending moment, due to lift, in the horizontal plane at x is

$$\left(M_{Z_1}\right)_L = -L(\ell + a - x)\cos\phi \tag{2b}$$

By using the usual elastic-beam theory and assuming small displacements, a condition of equilibrium can be expressed by the equation

$$EI_Z \frac{d^2y}{dx^2} = -M_{Z_1} = \left(L_\phi \phi_{x=\ell} + \phi D\right)(\ell + a - x) \qquad (0 \leq x \leq \ell) \tag{3}$$

where the load L, which simulates the lift force, has been assumed to be a linear function of the shaft twist (panel angle of attack) at the end of its flexible length. It has been assumed that the curvature in the XZ-plane is infinitely small and can be neglected in deriving equation (3).

The corresponding strain energy of the system in pure bending is found to be

$$U_B = \frac{1}{2EI_Z}\int_0^{\ell}\left[\left(L_\phi\phi_{x=\ell} + \phi D\right)(\ell + a - x)\right]^2 dx \tag{4}$$

and the strain energy in torsion is

$$U_\phi = \frac{C}{2}\int_0^{\ell}\left(\frac{d\phi}{dx}\right)^2 dx \tag{5}$$

where C is the torsional rigidity of the flexible shaft. Even though some small change in energy due to bending of the shaft in its plane (stiff direction) occurs, it is neglected in order to be consistent with the previous assumption of negligible curvature in this plane made in deriving the equilibrium equation. Therefore, the equation for the total increase in strain energy of the system is obtained from equations (4) and (5) and is

$$U_T = U_B + U_\phi \tag{6}$$

This total increase in strain energy for the divergence condition is equal to the decrease in potential of the system caused by the work done on the system by the externally applied loads.

The work done on the system by the drag load can be expressed as

$$\Omega_D = D\delta_D = D\left[\int_0^{\ell}(\ell + a - x)\frac{d^2y}{dx^2}\,\phi\,dx + \frac{b}{2}\left(\phi_{x=\ell}\right)^2\right] \tag{7}$$

where the first term on the right-hand side of the equation is the contribution to the work that is due to the change in potential of the drag load during lateral bending, and the second term is the contribution that is due to the change in potential of the drag load during rotation about the elastic axis.

Similarly, the work done on the system by the lift load can be expressed as

$$\Omega_L = \frac{L_\phi\phi_{x=\ell}}{2}\left[\phi_{x=\ell}\,d + \frac{1}{EI_Z}\int_0^{\ell}(\ell + a - x)^2\left(L_\phi\phi_{x=\ell} + \phi D\right)dx\right] \tag{8}$$

The total potential energy of the system is

$$V = U_T - \Omega_D - \Omega_L \tag{9}$$

Substituting the quantities given by equations (4) to (8), into equation (9) gives

$$V = \frac{1}{2EI_Z}\left\{\int_0^{l}\left[\left(L_\phi\phi_{x=l} + \phi D\right)(l + a - x)\right]^2 dx\right\} + \frac{C}{2}\int_0^{l}\left(\frac{d\phi}{dx}\right)^2 dx$$

$$- \frac{D}{EI_Z}\left[\int_0^{l}(l + a - x)^2\left(L_\phi\phi_{x=l} + \phi D\right)\phi\, dx + \frac{EI_Z b}{2}\left(\phi_{x=l}\right)^2\right]$$

$$- \frac{L_\phi\phi_{x=l}}{2}\left[\phi_{x=l}\, d + \frac{1}{EI_Z}\int_0^{l}(l + a - x)^2\left(L_\phi\phi_{x=l} + \phi D\right)dx\right] \qquad (10)$$

Theoretical Solution for the Divergence Condition

The theory of static divergence deals principally with the conditions under which equilibrium ceases to be stable. A system is in stable equilibrium if the value of its total potential energy is a relative minimum. The requirement for a multidegree-of-freedom system to be in equilibrium is that the first variation of its potential energy with respect to the generalized coordinates be equal to zero. Consequently, if the second variation of the potential energy with respect to the systems coordinates evaluated at the equilibrium position is greater than zero, the system is said to be in stable equilibrium (ref. 9). Therefore, defining the conditions under which equilibrium ceases to be stable (the static-divergence conditions) as those resulting when the second variation of the potential energy of the system is identically equal to zero, a divergence solution can be generated by

$$\frac{\partial^2 V}{\partial q_i^2} \equiv 0 \qquad (11)$$

In order to reduce the expression for the potential energy of the system (eq. (10)), the variable ϕ must be eliminated by expressing it as a function of x. Assume for ϕ a suitable function of x, which satisfies the boundary condition of the system. Let the mode

$$\phi = A\left[2\frac{x}{l + a} - \frac{x^2}{(l + a)^2}\right] \qquad (12)$$

be assumed to represent the deformed twisting mode shape and satisfy the boundary conditions of the following form:

$$\left.\begin{aligned} \phi &= 0 && (\text{at } x = 0)\\ \phi' &= K_1 A && (\text{at } x = 0)\\ \phi_{max} &= K_2 A && (\text{at } x = l)\\ \phi' &= K_3 A && (\text{at } x = l) \end{aligned}\right\} \qquad (13)$$

where K_1, K_2, and K_3 are constant quantities for a given model and loading configuration and do not need to be specifically known, and primed quantities represent derivatives with respect to x.

Substituting ϕ, as given by equation (12), and its derivatives into the expression for the potential energy of the system (eq. (10)) and performing the indicated integrations yields

$$V = \frac{-A^2}{2EI_Z}\left[B_1D^2 + L_\phi B_2 D + EI_Z\left(bD + L_\phi\, d\right)B_3\right] + 2CA^2B_4 \tag{14}$$

where

$$\left.\begin{aligned} B_1 &= \left[\frac{l^7}{7(l+a)^4} - \frac{l^6}{(l+a)^3} + \frac{13l^5}{5(l+a)^2} - \frac{3l^4}{l+a} + \frac{4l^3}{3}\right] \\ B_2 &= \left[\frac{l^7}{5(l+a)^4} - \frac{7l^6}{5(l+a)^3} + \frac{11l^5}{3(l+a)^2} - \frac{13l^4}{3(l+a)} + 2l^3\right] \\ B_3 &= \left[\frac{l^4}{(l+a)^4} - \frac{4l^3}{(l+a)^3} + \frac{4l^2}{(l+a)^2}\right] \\ B_4 &= \left[\frac{l^3}{3(l+a)^4} - \frac{l^2}{(l+a)^3} + \frac{l}{(l+a)^2}\right] \end{aligned}\right\} \tag{15}$$

The magnitude of the applied lift and drag forces at any given time are relatively dependent upon the dynamic pressure as follows:

$$q = \frac{L_\phi}{C_{L_\alpha} S} = \frac{D}{C_D S} \tag{16}$$

where

q	dynamic pressure
C_{L_α}	slope of lift curve
C_D	drag coefficient
S	reference (planform) area
L_ϕ	lift function

The problem has now reduced to solving for the minimum dynamic pressure necessary to generate the lift and drag forces which induce divergence. Accordingly, substituting equation (16) into equation (14) and taking the second variation of the resulting expression for the potential energy yields

$$\frac{\partial^2 V}{\partial A^2} = -\frac{1}{EI_Z}\left[\left(C_{L_\alpha} C_D B_2 + C_D{}^2 B_1\right) S^2 q^2 + EI_Z B_3 \left(C_D b + C_{L_\alpha} d\right) Sq\right] + 4CB_4 \tag{17}$$

Equating equation (17) to zero and solving the resulting quadratic equation in terms of the dynamic pressure, the critical dynamic pressure is found to be

$$q_{cr} = -\frac{C_1}{2}\frac{C_D b + C_{L_\alpha} d}{C_{L_\alpha} C_D C_4 + C_D{}^2 C_3} \pm \frac{1}{2}\left[\frac{C_1{}^2 \left(C_D b + C_{L_\alpha} d\right)^2}{\left(C_{L_\alpha} C_D C_4 + C_D{}^2 C_3\right)^2} + \frac{4C_2}{C_{L_\alpha} C_D C_4 + C_D{}^2 C_3}\right]^{1/2} \tag{18}$$

where

$$\left.\begin{aligned} C_1 &= \frac{EI_Z B_3}{S} \\ C_2 &= \frac{4CB_4 EI_Z}{S^2} \\ C_3 &= B_1 \\ C_4 &= B_2 \end{aligned}\right\} \tag{19}$$

Examination of the solution as given by equation (18), in terms of the critical dynamic pressure at divergence, shows that this solution is dependent only upon such static aerodynamic quantities as the drag coefficient $\left(C_D\right)$, the slope of the lift curve $\left(C_{L_\alpha}\right)$, the location of the lift and drag forces with respect to the elastic axis (d and b, respectively), and upon other known structural quantities as defined in the derivation (that is, the functions C_i).

Theoretical Solution for Drag Force Alone

The solution to the general analysis as given by equation (18) is only an approximation since it is dependent upon an assumed mode shape. The accuracy of the estimated divergence condition depends on how accurately the expression for the assumed mode shape represents the actual one that yields the minimum resistance to divergence. In order to assess the accuracy associated with the assumed mode given by equation (12), it is useful to examine a case that has been solved exactly by other investigators. Such a

case is divergence induced by a single applied load in the plane of the model, representing the drag force alone. The equation for the potential energy of this simplified case is given by equation (10) when L_ϕ is allowed to go to zero. Utilizing the assumed mode shape given by equation (12) in the new expression for the potential energy of the system and performing the indicated integrations yields

$$V = -\frac{A^2B_1}{2EI_Z}D^2 - \frac{bA^2B_3}{2}D + 2CA^2B_4 \tag{20}$$

By taking the second variation of this expression for the potential energy, equating it to zero, and solving the resulting quadratic equation, an estimate of the critical drag load associated with divergence can be determined. This critical drag load is

$$D_{cr} = -\frac{EI_Z b}{2}\frac{B_3}{B_1} \pm \frac{1}{2}\left[\left(EI_Z b\right)^2\left(\frac{B_3}{B_1}\right)^2 + 16EI_Z C\frac{B_4}{B_1}\right]^{1/2} \tag{21}$$

If the location of the applied single load is specified to be at the elastic-axis—root-chord junction (b and a are equal to zero), then equation (21) reduces to

$$D_{cr} = \pm 4.183\left(\frac{EI_Z C}{l^4}\right)^{1/2} \tag{22}$$

The exact differential equation of Timoshenko (ref. 10) for this same simplified case is

$$D_{cr} = \pm 4.03\left(\frac{EI_Z C}{l^4}\right)^{1/2} \tag{23}$$

A comparison of the coefficients of equations (22) and (23) indicates that the exact solution predicts a 4 percent lower critical drag load. As expected, the solution dependent upon the assumed mode predicts a higher value for the critical drag load since this mode does not offer the minimum resistance to divergence. However, it is concluded from this comparison that the assumed mode shape (given by eq. (12)) is sufficiently accurate for the purposes of the present investigation.

RESULTS AND DISCUSSION

Models

Experimental divergence data obtained for model configurations that are represented by the preceding analysis have been presented in references 6 and 7. In these references, the basic model configuration and the details of the individual models are also given. The basic model was a double-wedge control surface, with a wedge angle of 5° and the maximum thickness at the midchord as illustrated in figure 1. The rigid, unswept, square

planform was mounted on a flexible shaft; the pitch axis was at the 35-percent-chord line and the center of gravity was located at about the 53-percent-chord and 50-percent-span coordinates. The leading and trailing edges were circularly blunted and had radii of 6 percent of the chord. Since the models were essentially rigid, all deformations occurred in the flexible support shafts. Those parameters which define the structural characteristics of the model shafts are summarized in table I.

Experimental Data

For completeness, the basic data from the wind-tunnel tests obtained in helium (detailed in refs. 6 and 7) are summarized in table II. The test-section conditions and a velocity-index parameter $\frac{V}{\frac{c}{2}\omega_2\sqrt{\mu}}$ are listed for each test where divergence was observed. Presenting the divergence conditions in the form of the velocity-index parameter allows direct comparison between the variety of models having different levels of stiffness, since each is normalized by their particular level of stiffness. The experimental results from table II are presented in figure 3 as the variation of divergence velocity-index parameter with Mach numbers from 1.64 to 15.4.

An indication of the experimental "scatter" is shown at several Mach numbers where attempts were made to repeat a particular test. In most cases, the divergence was quite abrupt with the model striking the reflection plane less than 0.1 second after the first observable displacement.

Theoretical Investigation

Divergence due to lift only.- Figure 4 presents the results of an analytical effort to predict the experimental divergence. This investigation was accomplished by allowing the drag coefficient to go to zero in equation (17). The resulting expression was then equated to zero and solved. The solution, given in terms of critical dynamic pressure, is then dependent upon the lift-curve slope of the airfoil $\left(C_{L_\alpha}\right)$, the location of the lift force (a and b), and the torsional structural properties of the model shaft; therefore, being synonymous with the classical torsional divergence problem. The aerodynamic quantities were obtained by using simple Newtonian theory which is independent of Mach number $\left(C_p = 2 \sin^2\delta\right.$, where C_p is the pressure coefficient and δ is the local slope$\left.\right)$. While this theory predicts lift characteristics which are conservative for the lower Mach number range, it does predict the aerodynamic center to be located at about the 25-percent-chord station for a blunt-leading-edge double-wedge airfoil with a 5^o wedge angle near zero angle of attack. Other simple supersonic theories, such as piston theory, were not used since, in general, they apply to sharp-leading-edge airfoils and locate the aerodynamic center aft of the 35-percent-chord station; consequently, they predict no torsional

instability. It is worthy of note that the slope of the lift curve as predicted by Newtonian theory is the same as that predicted by third-order piston theory at $M = 7$ for similar double-wedge configurations but with sharp leading edges.

The poor prediction of the instability obtained by utilizing the classical torsional analysis is illustrated in figure 4. The prediction is shown as a ratio of average measured dynamic pressure to calculated dynamic pressures at divergence. For all models, the theory predicted dynamic pressures at divergence approximately four or five times greater than the average measured values over the entire Mach number range.

Divergence due to drag only.- Because of the poor agreement between the torsional divergence analysis and experimental results, an alternate divergence mechanism was sought. Some insight into the general character of the new type of divergence can be found in figure 5, which presents some typical examples of the model support shaft (with the control-surface panel removed) deformed by the divergence instability. The deformation is shown to consist of a lateral bending mode in addition to the torsional or twisting mode. This deformed mode combination and the relatively high magnitude of the aerodynamic drag loadings in comparison with the lift loadings for the blunt-leading-edge control surface suggested a general analysis including these parameters. (See section entitled "Divergence Analysis" for development.)

In order to determine the relative importance of high drag loadings on the systems stability, the critical conditions were calculated for the models of references 6 and 7 by utilizing the divergence theory pertaining to the drag-only case. The results are presented in figure 6 in the form of the ratio of average measured dynamic pressure to calculated dynamic pressure at divergence as a function of Mach number. The structural characteristics of each model tested were used in the analysis, with the drag load assumed to be acting at the midspan of the control surface at its leading edge. This assumption is reasonable since almost all the drag is due to the high pressure at the blunt leading edge of the control surface. The calculated dynamic pressure was obtained from equation (21) by using the relationship

$$q_{calc} = \frac{D_{cr}}{C_D S} \tag{24}$$

where the drag coefficient C_D is assumed to be constant over the entire Mach number range for the blunt airfoil shape. The resulting comparison in figure 6 shows that all the models tested at Mach numbers between 4 and 15 diverged while in a dynamic-pressure environment equal to approximately one-half that predicted by the drag-only divergence theory. The calculated results were even less encouraging for Mach numbers less than 4. However, at these lower speeds, the assumption of a constant drag coefficient is believed to be questionable and could, in part at least, account for the greater variance.

It is concluded from the results shown in figure 6 that the wind-tunnel tests are not adequately represented by the divergence theory including only the drag load. Furthermore, a comparison of figures 4 and 6 indicates that for the blunt control surfaces being investigated in this study, the drag load is a primary factor in their divergence.

Divergence including lift and drag loadings calculated from Newtonian theory.- The solution given by equation (18), which defines the critical value of the dynamic pressure associated with the case of two applied loads, depends on certain static aerodynamic quantities associated with the airfoil shape while operating in a given flow field. Such aerodynamic quantities as the drag coefficient C_D, the slope of the lift curve C_{L_α}, and the spanwise and chordwise locations of the two loads simulating the lift and drag forces with respect to the elastic axis are needed for the blunt double-wedge control surface over the Mach number range from 1.64 to 15.4. Therefore, the effect of these aerodynamic quantities on the divergence solution should be examined in order to be able to evaluate the possible variance in the general results when applying various aerodynamic theories.

The effect of the slope of the lift curve on the critical dynamic pressure associated with divergence is illustrated in figure 7. The critical dynamic pressure at angles of attack near zero are divided by the critical dynamic pressure for the divergence condition including only the drag load for the same model. The model under consideration has an aluminum-alloy shaft 5 inches long (12.7 cm), 1.2 inches wide (3.1 cm), and 0.065 inch thick (0.165 cm), with the lift acting at the elastic axis and the drag acting at the control-surface leading edge. The drag coefficient was given a constant value of 0.284 based on the planform area. The critical dynamic pressure is seen to decrease with an increase in C_{L_α}. For a value of $C_{L_\alpha} = 0.6$ (the calculated value from Newtonian theory – which is realistic for the higher Mach numbers), the critical dynamic pressure is reduced about 36 percent from that of the drag-only case.

Figure 8 presents resulting critical dynamic pressures for the same model configuration when the lift load is applied at various chordwise positions forward $\left(+\frac{d}{l}\right)$ and aft $\left(-\frac{d}{l}\right)$ of the elastic axis. As would be expected, moving the location of the lift load aft of the elastic axis is stabilizing and moving it forward of the elastic axis is destabilizing. For a constant value of C_{L_α}, the variation in the critical dynamic pressure is only between 5 and 10 percent when d/l changes from 0 to ± 0.80. This small variation is in contrast to that obtained for the classical torsional divergence instability where the divergence condition is directly proportional to the chordwise location of the lift force.

For completeness, the critical dynamic pressure as a function of drag coefficient is shown in figure 9 for constant values of C_{L_α}, a/l, and d/l. It is realized that the drag coefficient is nearly constant for a given configuration at supersonic and hypersonic speeds. However, because of the prime effect that drag has on the stability of the system

under investigation, if there is a variation in drag coefficient, it is important. For example, if at the low supersonic speeds there is a 25-percent change in C_D, a 15-percent change in the critical dynamic pressure would result, other quantities remaining unchanged.

The final parameter to be examined is the chordwise location of drag load, or the distance the drag load is acting forward $\left(+\frac{b}{l}\right)$ or aft $\left(-\frac{b}{l}\right)$, of the elastic axis. The critical dynamic pressure as a function of this applied load position is presented in figure 10. Again, as would be expected, a decrease in stability is obtained by applying the drag load forward of the elastic axis and, conversely, an increase in stability is obtained by applying the drag load aft of the elastic axis. Results from calculations not shown in figure 10 indicate that for the range of structural characteristics of the models of the experimental program, the percent increase or decrease in stability resulting from applying the load off the elastic axis is a constant for corresponding loading positions on all the models. It can be concluded from the results presented in figures 8 and 10 that the locations of the applied forces are of only secondary importance to the divergent condition, since in both cases there is only a maximum of about 10-percent change in the divergence results.

Ratios of the average measured values of dynamic pressure (from the experimental wind-tunnel programs of refs. 6 and 7) to the calculated values are presented as a function of Mach number in figure 11. Newtonian theory was used to determine the static aerodynamic quantities needed to obtain a closed-form solution to equation (18). Solutions to the divergence problem including both lift and drag loadings are indicated in the figure by the solid circular symbols. Over the low supersonic speed range, the calculated results are unconservative up to a Mach number of 3, whereupon they become conservative with further increase in Mach number. However, the calculated values do tend to approach the measured values of dynamic pressure of the divergence instability at the very high Mach numbers.

Divergence including measured lift and drag loads.- More accurate analytical prediction of the measured divergence results of the wind-tunnel tests over the entire Mach number range would require measured static aerodynamic characteristics for the particular blunt-leading-edge control surface under consideration. Unfortunately, experimentally determined quantities such as these do not seem to exist in the literature for this configuration. These quantities, therefore, have been obtained in helium at Mach 6.8 and 15.4 in the Langley hypersonic aeroelasticity tunnels. Normal static aerodynamic derivative measurements using six-component strain-gage balances were obtained. The data from these tests are presented in figure 12 in the form of the lift coefficient, the drag coefficient, and the location of the aerodynamic center – all as functions of angle of attack. From these experimental results, it can be determined that near zero angle of attack the aerodynamic characteristics of a blunt, double-wedge airfoil having a leading-edge radius equal to 6 percent chord are as follows:

At M = 15.4	At M = 6.8	Newtonian theory
$C_{L_\alpha} = 0.60$	$C_{L_\alpha} = 0.53$	$C_{L_\alpha} = 0.606$
$C_D = 0.168$	$C_D = 0.127$	$C_D = 0.161$
$x_o/c = 0.325$	$x_o/c = 0.252$	$x_o/c = 0.220$

Mentioned here for interest, the comparable aerodynamic characteristics for a sharp-leading-edge, double-wedge airfoil are as follows:

At M = 15.4	At M = 6.8	Newtonian theory
$C_{L_\alpha} = 0.69$	$C_{L_\alpha} = 0.55$	$C_{L_\alpha} = 0.679$
$C_D = 0.008$	$C_D = 0.006$	$C_D = 0.00134$
$x_o/c = 0.315$	$x_o/c = 0.315$	$x_o/c = 0.250$

These results indicate that the drag loading is increased by a factor of about 20 when a sharp-leading-edge configuration is blunted to a configuration with a radius equal to 6 percent of its chord, the length of the chord being held constant.

Incorporating the measured aerodynamic coefficients and aerodynamic-center location obtained at Mach 6.8 and 15.4 for the blunt airfoil into the divergence analysis yielded the results illustrated in figure 11 by the open circular symbols. The agreement between the measured and calculated dynamic pressure for divergence is seen to be excellent. Also shown in figure 11 for comparison are the measured to calculated results from figures 4 and 6 where the analysis included the lift and drag loadings independently. This comparison reiterates that the experimental divergence encountered by the blunt airfoil model-shaft configuration being investigated was quite different from the classical torsional divergence attributed to lift loadings. The new type of divergence consists of a combination twisting-bending mode which is highly sensitive to drag loadings, and consequently produces a much lower stability boundary for the configuration over the entire Mach number range of this investigation.

CONCLUSIONS

An investigation of the divergence characteristics of some rigid all-movable control surfaces supported by a flexible shaft has been conducted. The particular configuration studied was a blunt, double-wedge control surface with a 5^o wedge angle and a leading-edge radius of 6 percent chord. The control surface was supported by a relatively long, thin rectangular shaft that was weak in the lift direction and stiff in the drag direction. The results of the study indicated the following conclusions:

1. A new type of divergence instability is inherent to this configuration. It is characterized by a mode of deflection consisting of lateral bending and torsional rotation.

2. The two-degree-of-freedom instability can result in a lower divergence boundary than the classical torsional divergence case. This fact was exhibited for the series of models of this investigation, both analytically and experimentally, over the Mach number range from 1.64 to 15.4.

3. Estimates obtained from a potential-energy analysis, using aerodynamic characteristics predicted by simple Newtonian theory, were in fair agreement with experimental results for the Mach number range from 1.64 to 15.4. It was found that inclusion of the drag loadings was essential to predicting the divergence instability.

4. Since there is a dearth of experimental verification of the aerodynamic theories for blunt control surfaces, it was found necessary to measure the static aerodynamic characteristics for the configuration being studied in order to predict the divergence condition precisely. These parameters were measured at Mach 6.8 and 15.4, and incorporating the results into the divergence analysis afforded excellent divergence predictions.

Langley Research Center,
National Aeronautics and Space Administration,
Langley Station, Hampton, Va., May 29, 1968,
126-14-02-08-23.

REFERENCES

1. Scanlan, Robert H.; and Rosenbaum, Robert: Introduction to the Study of Aircraft Vibration and Flutter. The Macmillan Co., 1951.

2. Bisplinghoff, Raymond L.; Ashley, Holt; and Halfman, Robert L.: Aeroelasticity. Addison-Wesley Pub. Co., Inc., c.1955.

3. Lauten, William T., Jr.; Levey, Gilbert M.; and Armstrong, William O.: Investigation of an All-Movable Control Surface at a Mach Number of 6.86 for Possible Flutter. NACA RM L58B27, 1958.

4. Morgan, Homer G.; and Miller, Robert W.: Flutter Tests of Some Simple Models at a Mach Number of 7.2 in Helium Flow. NASA MEMO 4-8-59L, 1959.

5. Miller, Robert W.; and Hannah, Margery E.: Flutter Investigation of 60° to 80° Delta-Planform Surfaces at a Mach Number of 7.0. NASA TM X-325, 1960.

6. Hanson, Perry W.: Aerodynamic Effects of Some Configuration Variables on the Aeroelastic Characteristics of Lifting Surfaces at Mach Numbers From 0.7 to 6.86. NASA TN D-984, 1961.

7. Goetz, Robert C.: Effects of Leading-Edge Bluntness on Flutter Characteristics of Some Square-Planform Double-Wedge Airfoils at a Mach Number of 15.4. NASA TN D-1487, 1962.

8. Goetz, Robert C.: Effects of Leading-Edge Sweep on Flutter Characteristics of Some Delta-Planform Surfaces at a Mach Number of 15.4. NASA TN D-2360, 1964.

9. Langhaar, Henry L.: Energy Methods in Applied Mechanics. John Wiley & Sons, Inc., c.1962.

10. Timoshenko, S.: Theory of Elastic Stability. McGraw-Hill Book Co., Inc., 1936.

TABLE I.- MODEL SHAFT CHARACTERISTICS

[Refs. 6 and 7]

Model	Thickness, t		Length, l		I_Z		C	
	in.	cm	in.	cm	in^4	cm^4	$lb\text{-}in^2$	$N\text{-}m^2$
h = 0.750 in. (1.905 cm); a = 2.0 in. (5.08 cm); S = 16 in^2 (103 cm^2); E = 30×10^6 lb/in^2 (207 GN/m^2); G = 11.4×10^6 lb/in^2 (78.6 GN/m^2)								
6-20-65	0.065	0.1651	2.0	5.08	17.16×10^{-6}	7.14×10^{-4}	739.948	2.1303
6-20-47	.047	.1194	2.0	5.08	6.49×10^{-6}	2.70×10^{-4}	284.206	.8196
6-20-33	.033	.0838	2.0	5.08	2.24×10^{-6}	$.932 \times 10^{-4}$	99.585	.2867
h = 1.200 in. (3.048 cm); a = 3.0 in. (7.62 cm); S = 36 in^2 (232 cm^2); E = 10×10^6 lb/in^2 (68.9 GN/m^2); G = 3.8×10^6 lb/in^2 (26.2 GN/m^2)								
6-A-6-1	0.065	0.1651	5.0	12.70	27.46×10^{-6}	11.43×10^{-4}	1209.587	3.4824
6-A-6-2	.065	.1651	6.0	15.24	27.46×10^{-6}	11.43×10^{-4}	1209.587	3.4824
6-A-6-4	.065	.1651	4.0	10.16	27.46×10^{-6}	11.43×10^{-4}	1209.587	3.4824

TABLE II.- EXPERIMENTAL DIVERGENCE RESULTS

Model	M	ρ		Speed of sound		q		$\frac{v}{\frac{c}{2}\omega_2\sqrt{\mu}}$
		$slugs/ft^3$	kg/cm^3	ft/sec	m/sec	lb/ft^2	N/m^2	
6-20-65-1	1.64	0.001526	0.786468	920	280.4	1728	82 737	1.13
6-20-47-1	2.00	.000500	.257689	859	261.8	732	35 048	1.18
6-20-65-2	2.55	.001182	.609178	760	231.6	2218	106 198	1.24
6-20-65-6	2.55	.001215	.626185	752	229.2	2230	106 773	1.29
6-20-47-3	3.00	.000423	.218005	702	214.0	939	44 960	1.33
6-20-33-1	3.98	.000132 to .000151	.068030 to .077822	582	177.4	353 to 403	16 902 to 19 296	1.44 to 1.34
6-20-47-2	6.83	.000067 to .000068	.034530 to .035046	870	265.2	1180 to 1200	56 499 to 57 456	1.48
6-A-6-1	15.20	.0000136	.007009	431	131.4	292	13 981	1.37
6-A-6-2	15.00	.0000096	.004948	408	124.4	180	8 618	1.12
6-A-6-4	15.35	.0000226	.011648	395	120.4	415	19 870	1.07

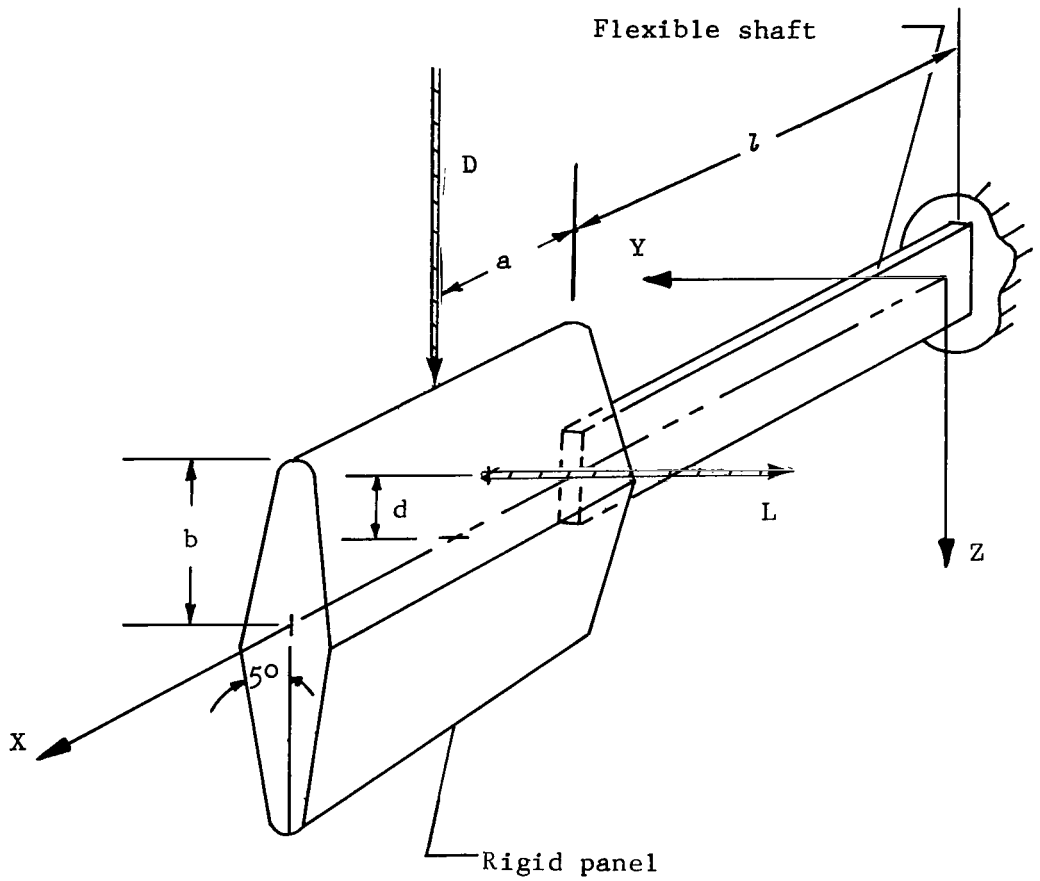

Figure 1.- Model configuration. Fixed coordinate system.

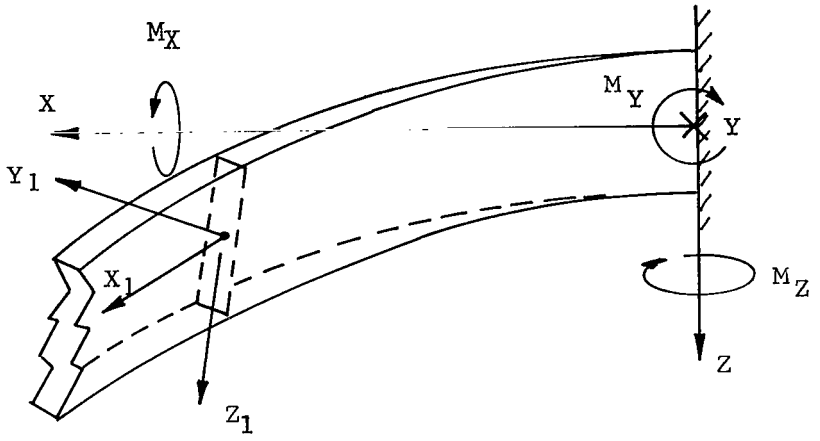

(a) x_1, y_1, z_1 coordinate system.

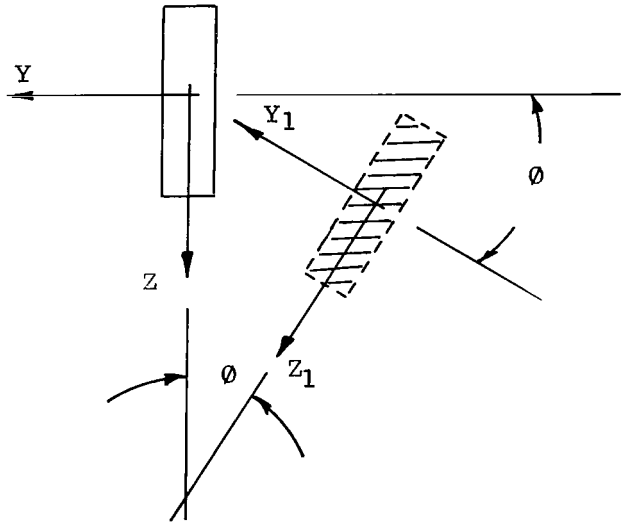

(b) Arbitrary cross section.

Figure 2.- Deformed shaft configuration.

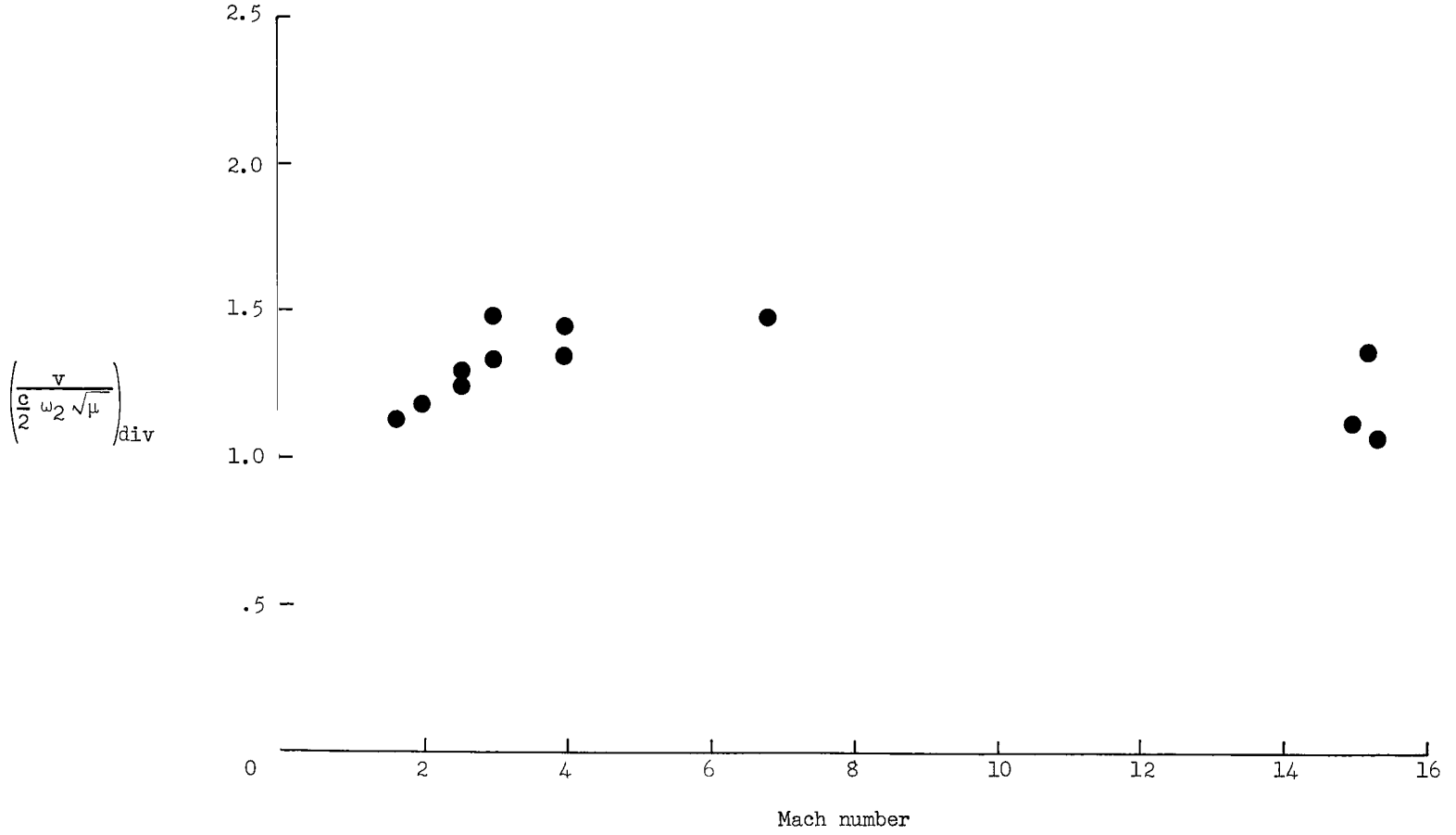

Figure 3.- Experimental divergence characteristics of blunt, double-wedge control surface having a leading-edge radius equal to 6 percent of its chord (refs. 6 and 7).

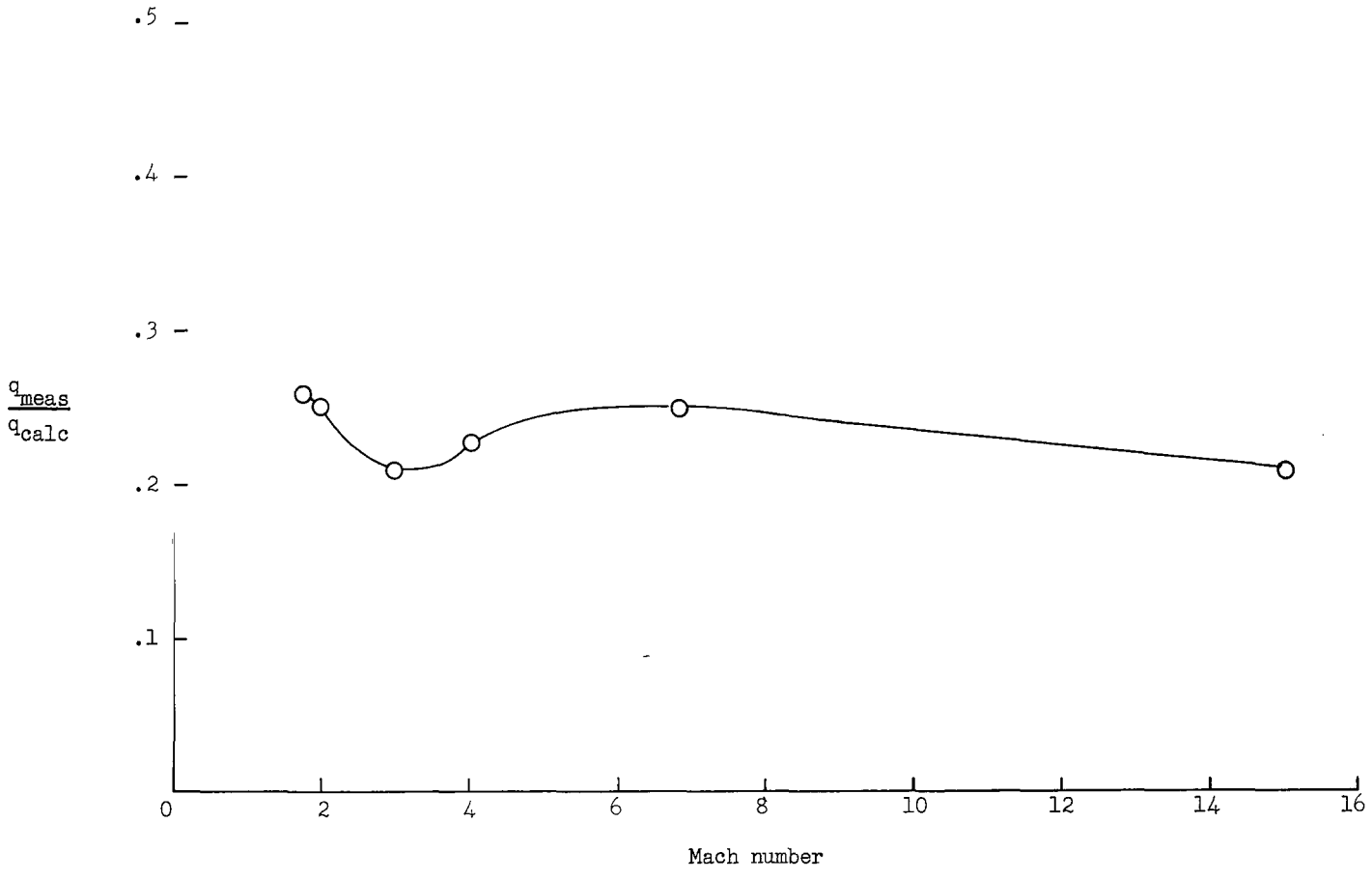

Figure 4.- Comparison of measured dynamic pressure at divergence with calculated values including only the lift force.

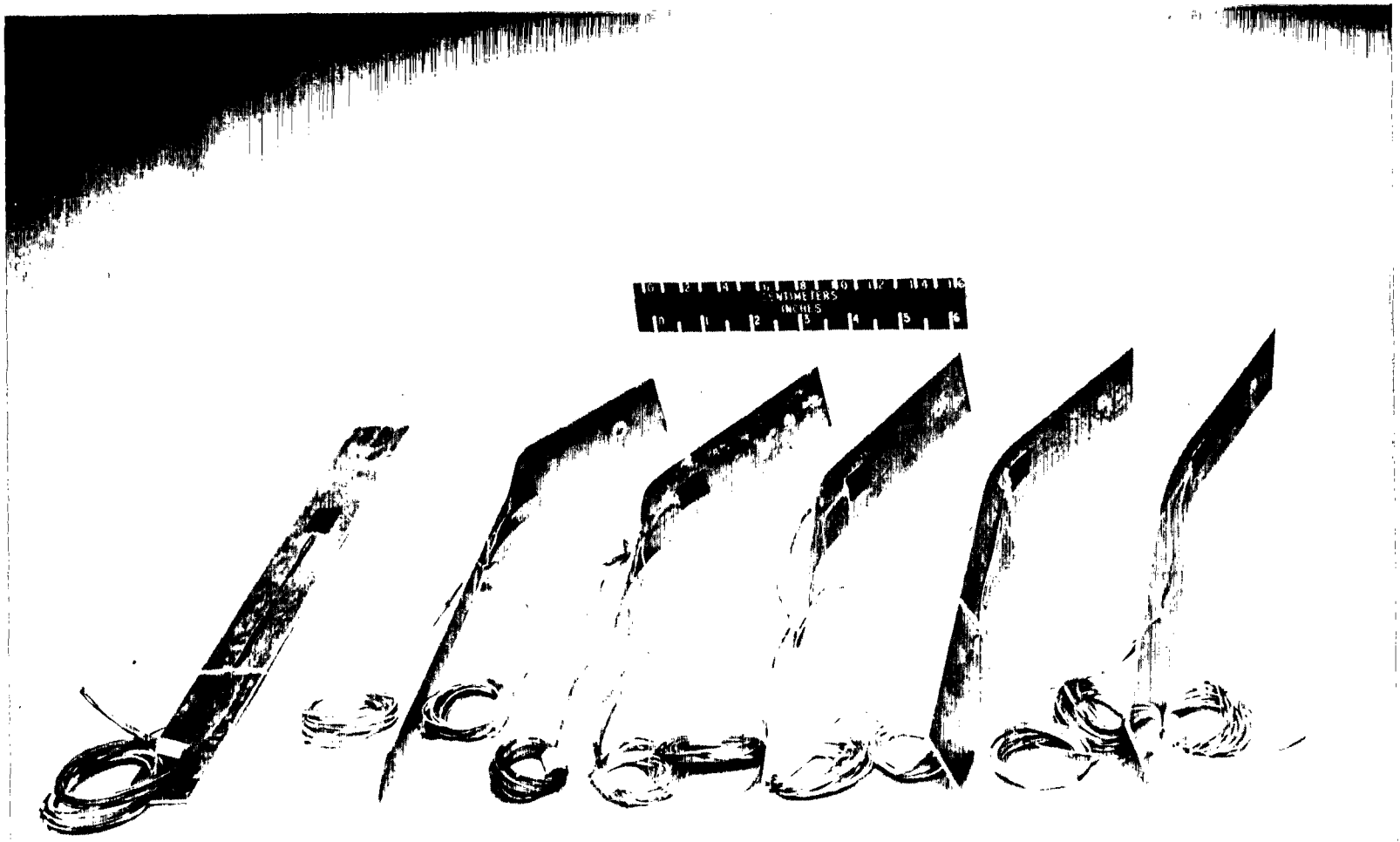

Figure 5.- Comparison between typical deformed and undeformed model shafts.

L-66-9852.1

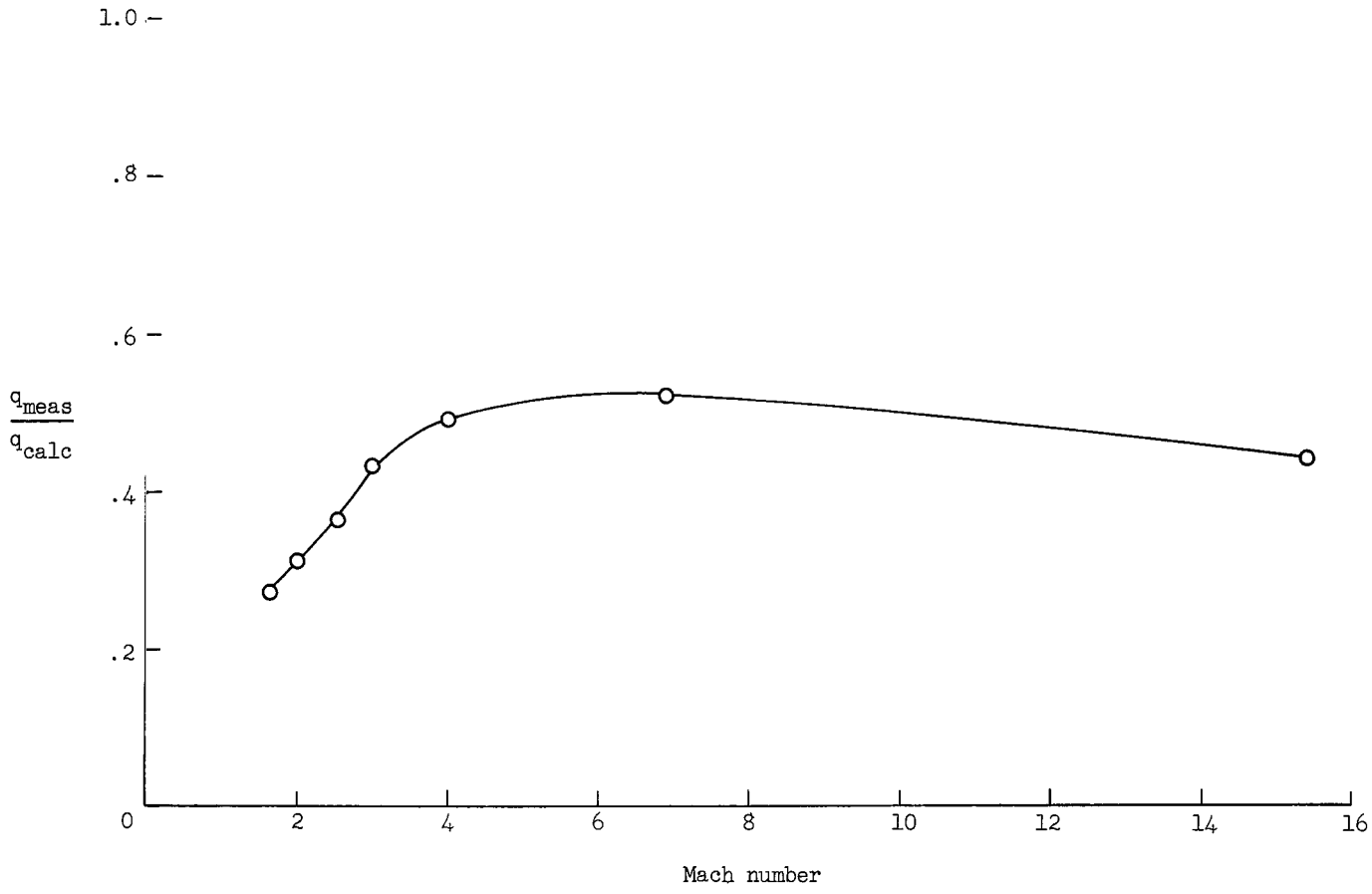

Figure 6.- Comparison of measured dynamic pressure at divergence with calculated values including only the drag load.

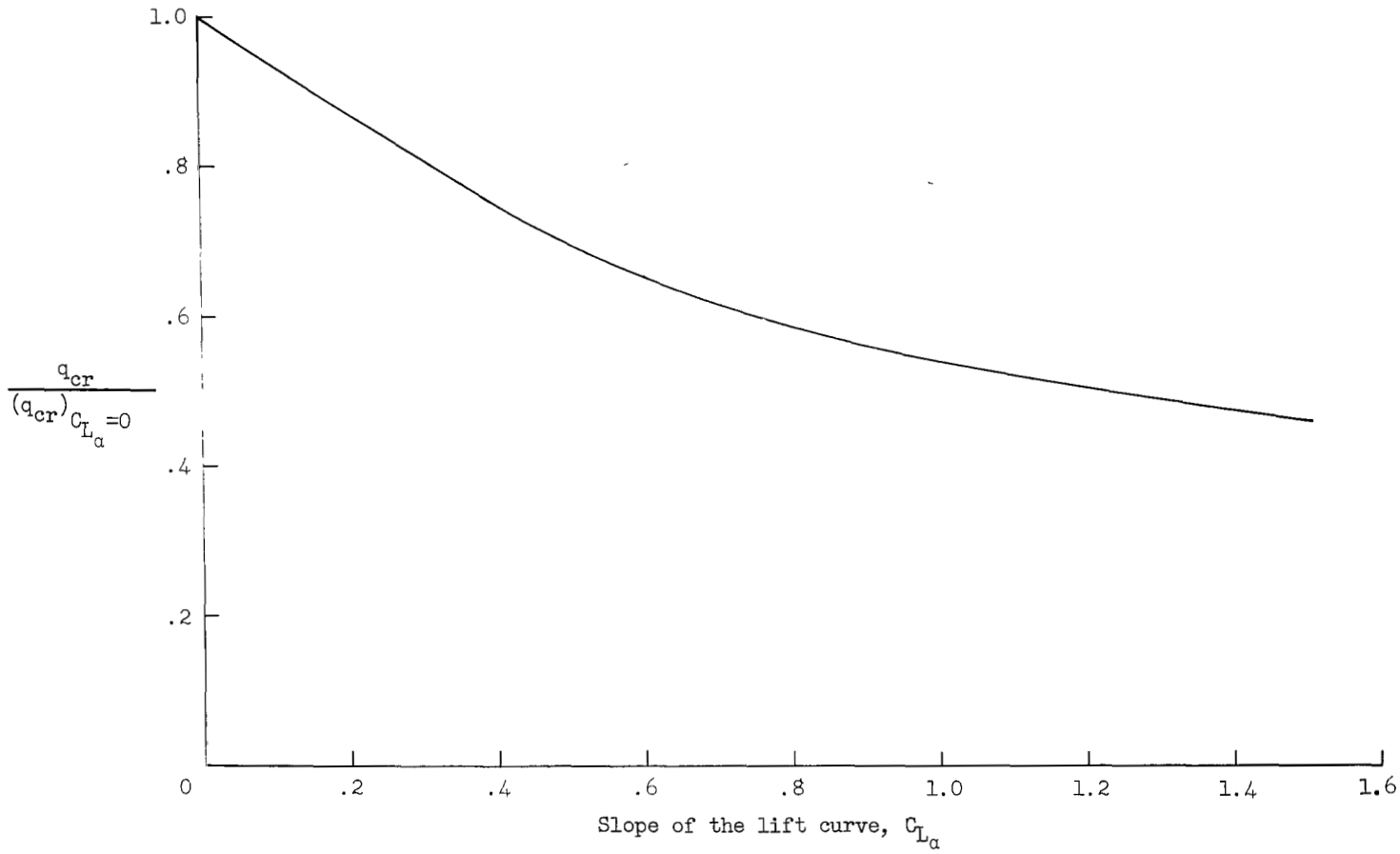

Figure 7.- Analytical effect of the slope of the lift curve on the critical dynamic pressure. $a/l = 0.6$; $d/l = 0$; $b/l = 0.42$; $C_D = 0.284$.

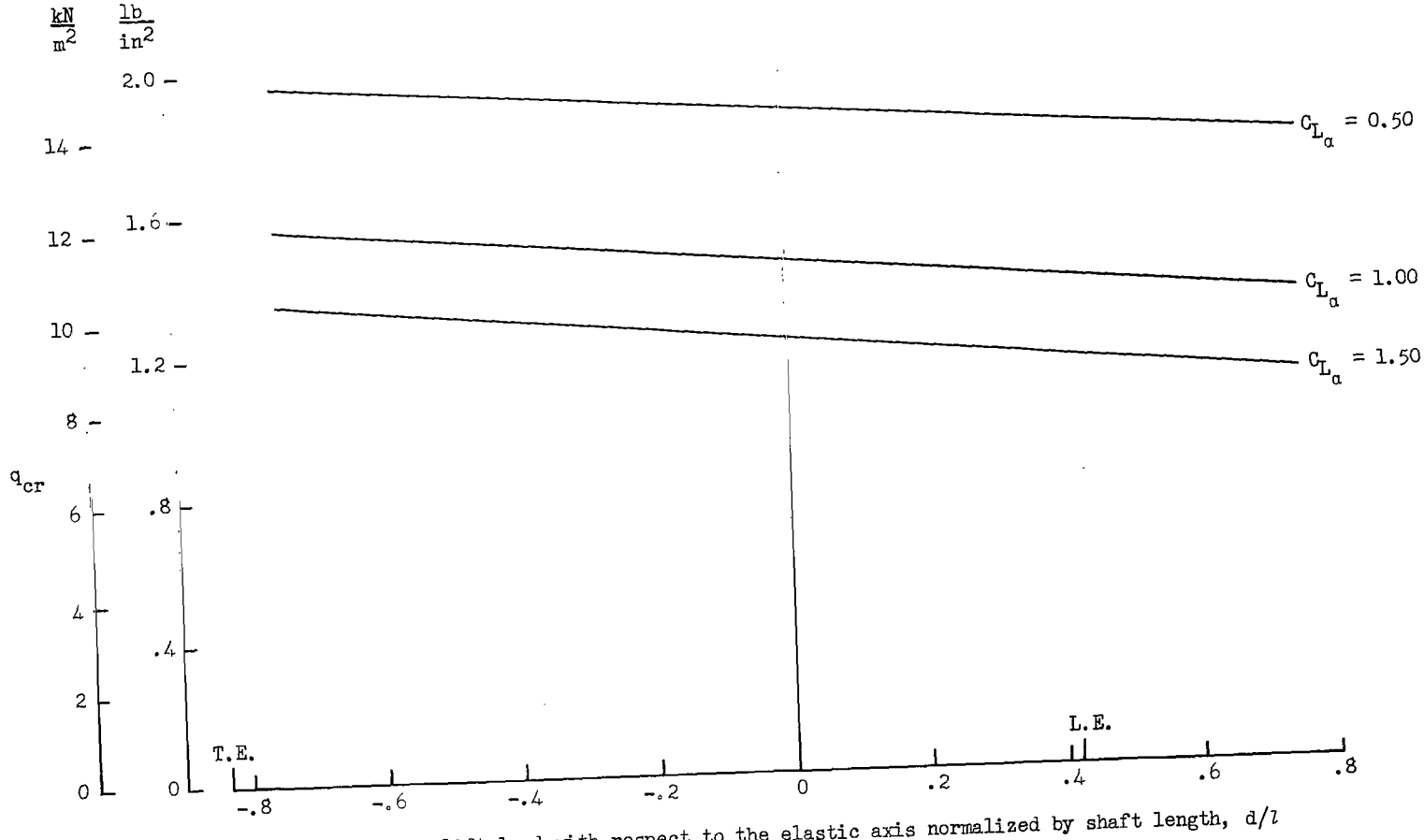

Figure 8.- Analytical effect of the chordwise location of lift load on the critical dynamic pressure. $a/l = 0.60$; $b/l = 0.42$; $C_D = 0.284$.

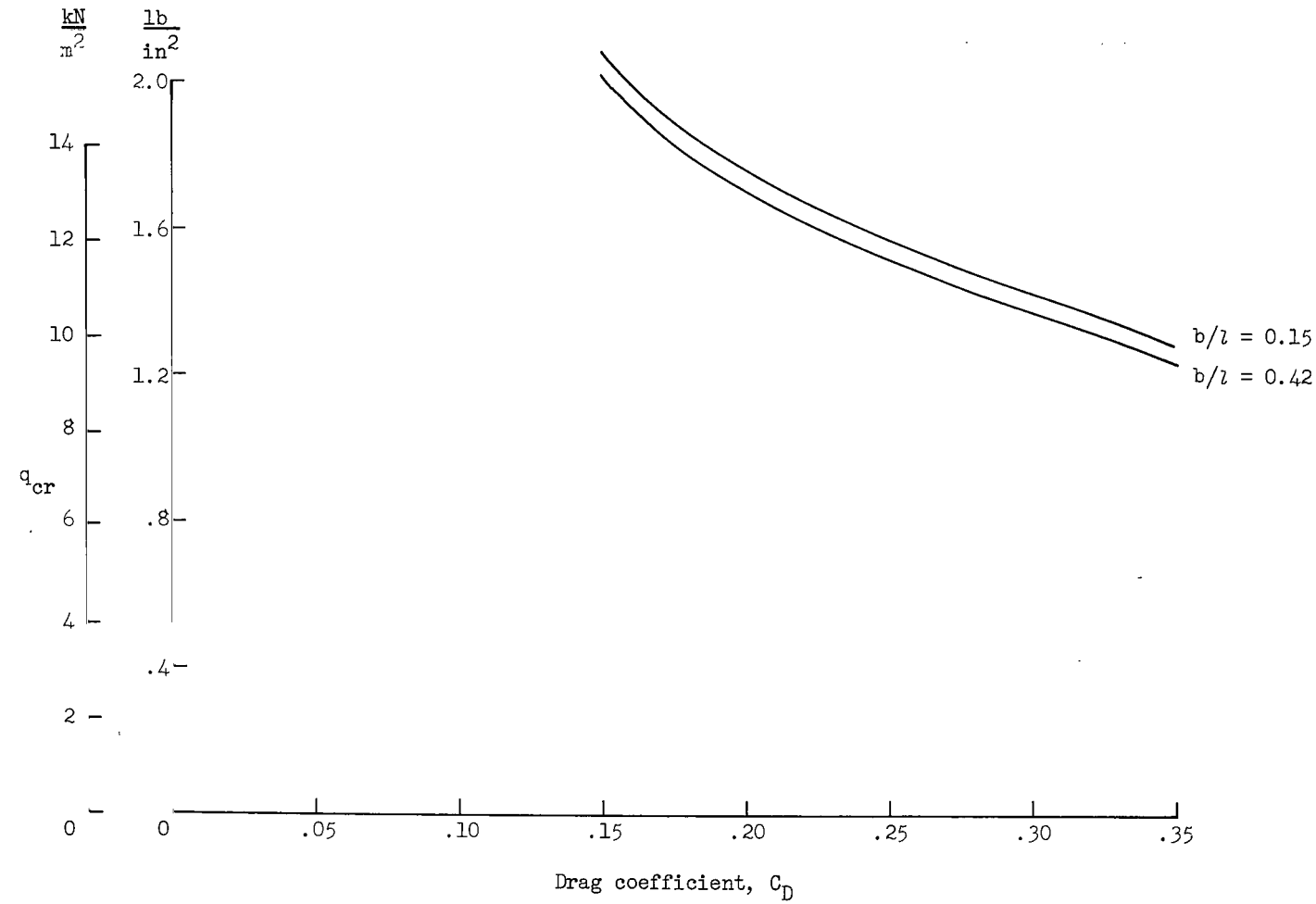

Figure 9.- Analytical effect of the drag coefficient on the critical dynamic pressure. $a/l = 0.60$; $d/l = +0.051$; $C_{L_\alpha} = 1.00$.

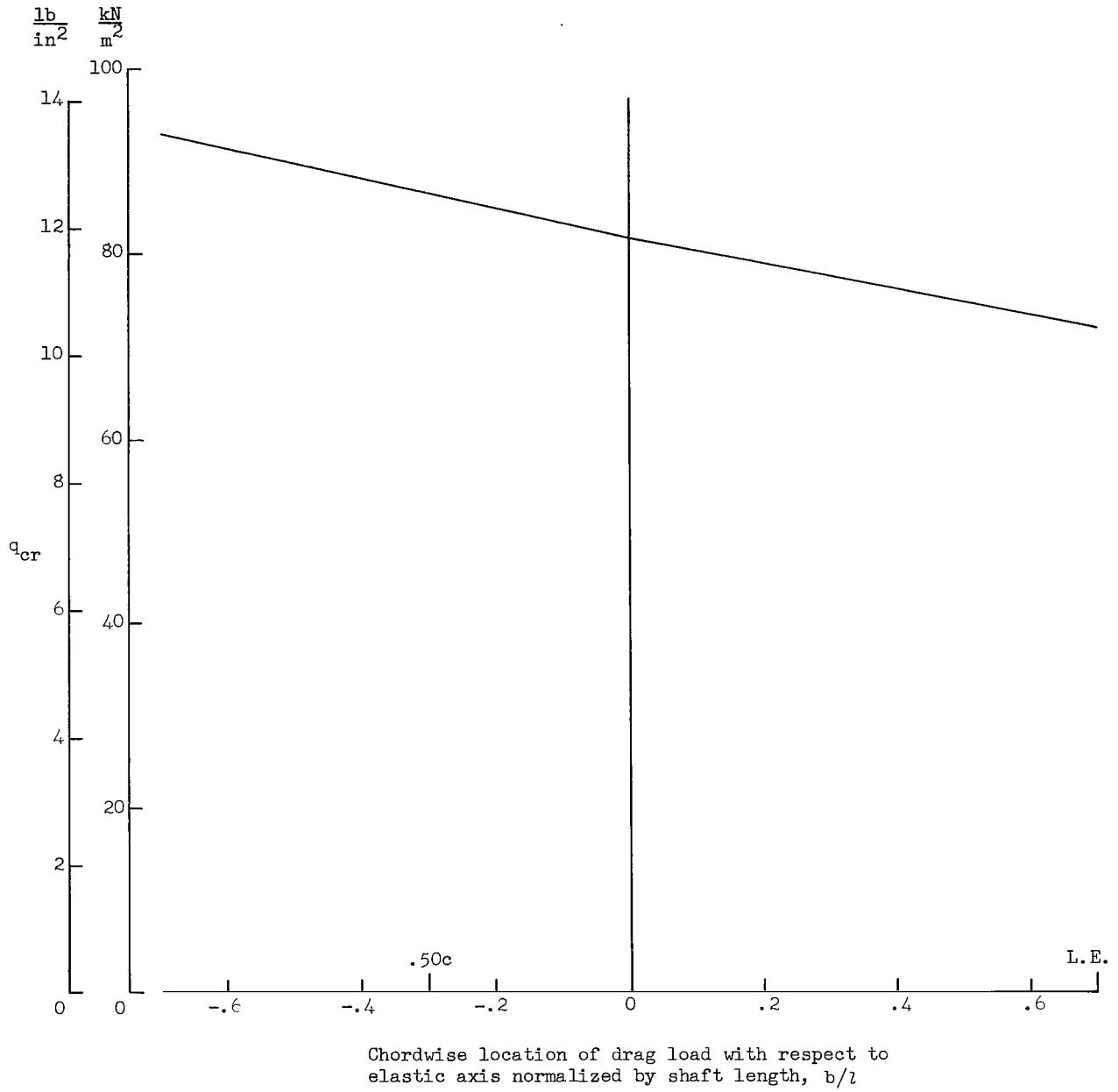

Figure 10.- Analytical effect of the chordwise location of the drag load on the critical dynamic pressure. $a/l = 1.00$; $d/l = 1.00$; $C_D = 0.13$; $C_{L_\alpha} = 0.55$.

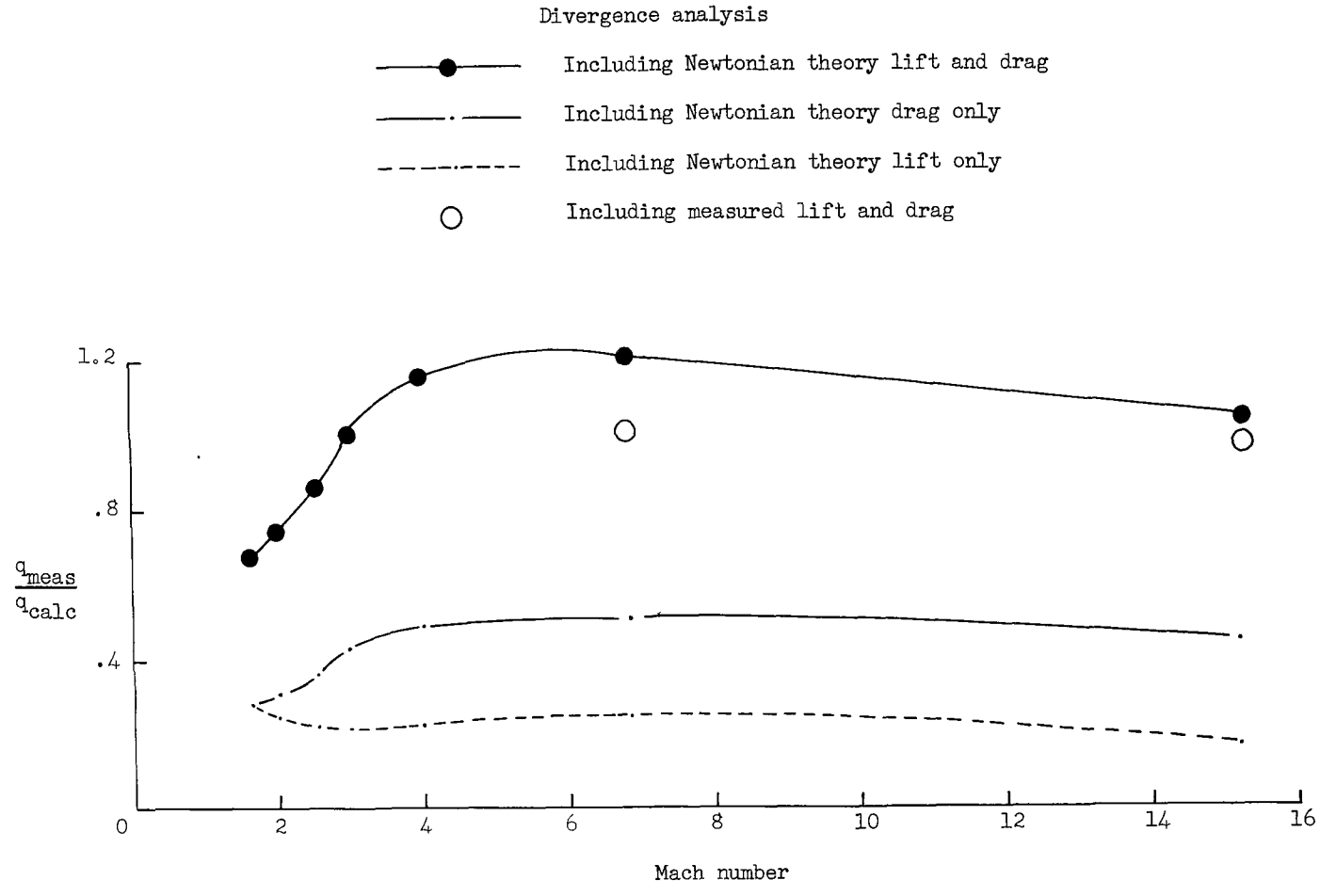

Figure 11.- Comparison of the measured dynamic pressure at divergence with calculated values.

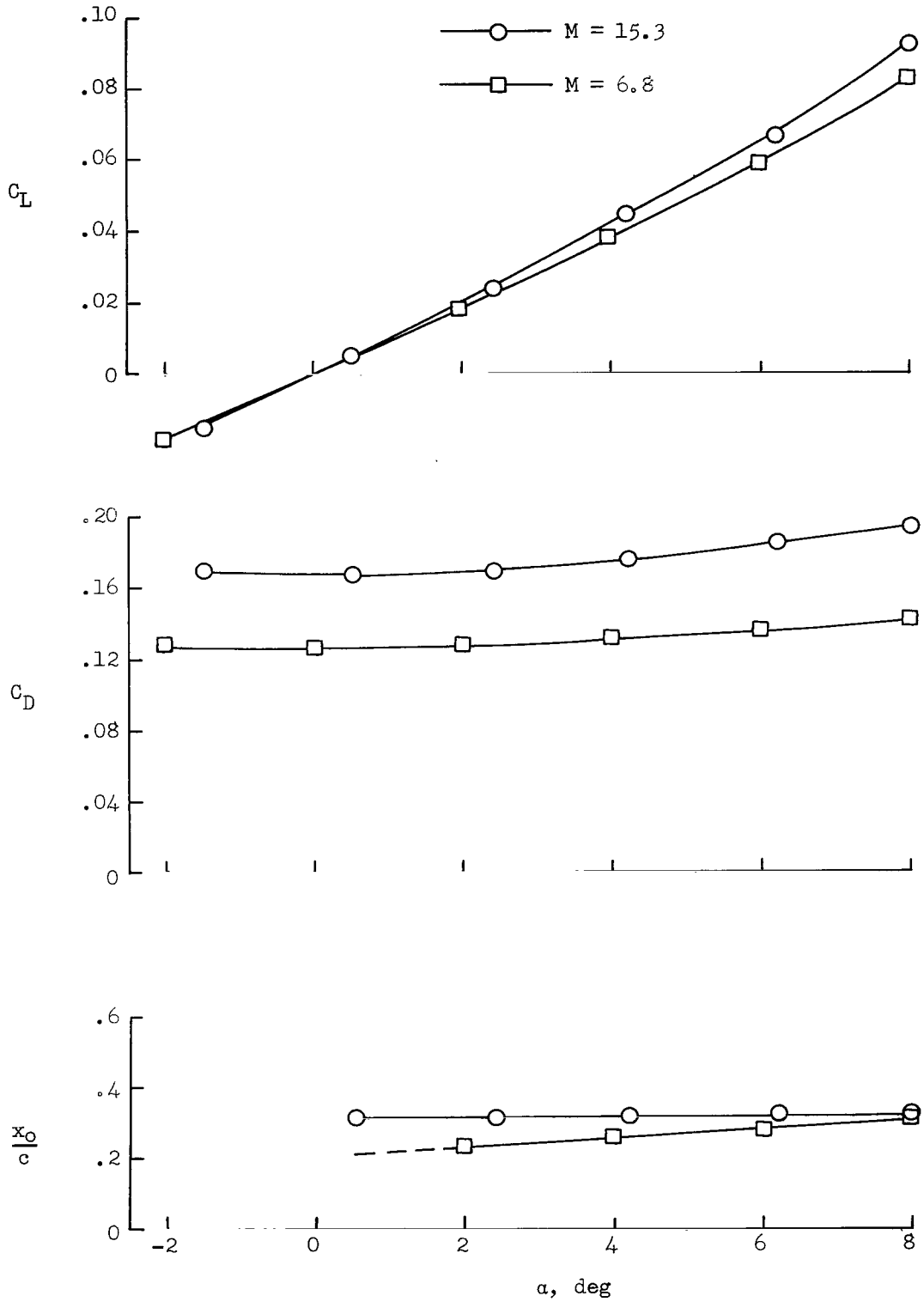

Figure 12.- Characteristics of a blunt, symmetrical, double-wedge airfoil having a leading-edge radius equal to 6 percent of its chord.

NATIONAL AERONAUTICS AND SPACE ADMINISTRATION
WASHINGTON, D. C. 20546

OFFICIAL BUSINESS

FIRST CLASS MAIL

POSTAGE AND FEES PAID
NATIONAL AERONAUTICS AND
SPACE ADMINISTRATION

POSTMASTER: If Undeliverable (Section 158 Postal Manual) Do Not Return

"The aeronautical and space activities of the United States shall be conducted so as to contribute . . . to the expansion of human knowledge of phenomena in the atmosphere and space. The Administration shall provide for the widest practicable and appropriate dissemination of information concerning its activities and the results thereof."

—NATIONAL AERONAUTICS AND SPACE ACT OF 1958

NASA SCIENTIFIC AND TECHNICAL PUBLICATIONS

TECHNICAL REPORTS: Scientific and technical information considered important, complete, and a lasting contribution to existing knowledge.

TECHNICAL NOTES: Information less broad in scope but nevertheless of importance as a contribution to existing knowledge.

TECHNICAL MEMORANDUMS: Information receiving limited distribution because of preliminary data, security classification, or other reasons.

CONTRACTOR REPORTS: Scientific and technical information generated under a NASA contract or grant and considered an important contribution to existing knowledge.

TECHNICAL TRANSLATIONS: Information published in a foreign language considered to merit NASA distribution in English.

SPECIAL PUBLICATIONS: Information derived from or of value to NASA activities. Publications include conference proceedings, monographs, data compilations, handbooks, sourcebooks, and special bibliographies.

TECHNOLOGY UTILIZATION PUBLICATIONS: Information on technology used by NASA that may be of particular interest in commercial and other non-aerospace applications. Publications include Tech Briefs, Technology Utilization Reports and Notes, and Technology Surveys.

Details on the availability of these publications may be obtained from:

SCIENTIFIC AND TECHNICAL INFORMATION DIVISION

NATIONAL AERONAUTICS AND SPACE ADMINISTRATION

Washington, D.C. 20546